Structural insight into tanapoxvirus mediated inhibition of apoptosis

Chathura D. Suraweera[1], Mohd Ishtiaq Anasir[1$], Srishti Chugh[1&], Airah Javorsky[1], Rachael E. Impey[1], Mohammad Hasan Zadeh[1], Tatiana P. Soares da Costa[1], Mark G. Hinds[2*] and Marc Kvansakul[1*]

[1]La Trobe Institute for Molecular Science, Department of Biochemistry and Genetics, La Trobe University, VIC 3086, Australia

[2]Bio21 Molecular Science and Biotechnology Institute, The University of Melbourne, Parkville, Australia

[&]Current address: CSL Limited, Parkville, Victoria, Australia

[$]Current address: Centre for Virus and Vaccine Research, Sunway University, Malaysia

Running title: Tanapoxvirus 16L inhibits apoptosis

Keywords: Poxvirus, tanapoxvirus, apoptosis, X-ray crystallography, isothermal titration calorimetry, Bcl-2

ABSTRACT

Premature programmed cell death or apoptosis of cells is a strategy utilized by multicellular organisms to counter microbial threats. Tanapoxvirus (TPV) is a large double-stranded DNA virus belonging to the *poxviridae* that causes mild Monkeypox-like infections in humans and primates. TPV encodes for a putative apoptosis inhibitory protein 16L. We now show that TPV16L is able to bind to a range of peptides spanning the BH3 motif of human pro-apoptotic Bcl-2 proteins, and is able to counter growth arrest of yeast induced by human Bak and Bax. We then determined the crystal structures of TPV16L bound to three identified interactors, Bax, Bim and Puma BH3. TPV16L adopts a globular Bcl-2 fold comprising 7 α-helices, and utilizes the canonical Bcl-2 binding groove to engage pro-apoptotic host cell Bcl-2 proteins. Unexpectedly, TPV16L is able to adopt both a monomeric as well as a domain-swapped dimeric topology where the α1 helix from one protomer is swapped into a neighbouring unit. Despite adopting two different oligomeric forms, the canonical ligand binding groove in TPV16L remains unchanged from monomer to domain-swapped dimer. Our results provide a structural and mechanistic basis for tanapoxvirus mediated inhibition of host cell apoptosis, and reveal the capacity of Bcl-2 proteins to adopt differential oligomeric states whilst maintaining the canonical ligand binding groove in an unchanged state.

Introduction

Tanapoxvirus [1] is a member of the *yatapoxviridae*, a large double-stranded DNA virus from the *poxviridae* superfamily. The *yatapoxviridae* comprise Tanapox virus (TPV), Yaba-like disease virus (YLDV) and Yaba monkey tumor virus (YMTV), and causes mild monkeypox-like infections in humans as well as primates with symptoms that include fever and skin lesions [2]. Tanapoxvirus encodes a range of immune modulatory proteins such as TNF inhibitors [3], as well as a putative B-cell lymphoma-2 (Bcl-2) homolog [4]. Bcl-2 proteins constitute a large family of proteins that primarily control programmed cell death, or apoptosis, in higher organisms [5] and are evolutionarily ancient [6]. The family comprises both prosurvival and proapoptotic members, which are characterized by the presence of one or more of four Bcl-2 homology or BH motifs and a transmembrane anchor region [7]. The mammalian prosurvival Bcl-2 members comprise Bcl-2, Bcl-w, Bcl-x_L, Mcl-1, A1 and Bcl-b, and maintain host cell survival. In contrast, proapoptotic Bcl-2 family members are subdivided into two separate groups, the multimotif executors that comprise Bak, Bax and Bok, and a second group, the BH3-only proteins, which only feature a BH3 motif and includes Bad, Bid, Bik, Bim, Bmf, Hrk, Noxa, and Puma [8]. The BH3-only proteins modulate apoptosis by neutralizing the activity of prosurvival Bcl-2 through binding a surface groove [9]. After activation, Bak and Bax oligomerize to perforate the outer mitochondrial membrane leading to inner membrane herniation [10] and subsequent release of cytochrome *c*, that triggers the formation of the apoptosome and activation of downstream caspases that dismantle the cell [11].

A number of large DNA viruses encode functional, sequence and structural homologs of Bcl-2 that promote infected host cell survival and viral proliferation [12]. Viral Bcl-2 homologs have been identified in *herpesviridae*, include those from Epstein Barr virus BHRF1 [13, 14] and Kaposi sarcoma virus KsBcl-2 [15-17]. Other major virus families that

contain members encoding for pro-survival Bcl-2 proteins include the *asfarviridae* with African swine fever virus encoded A179L [18-20], and grouper iridovirus encoded GIV66 [21, 22] from the *iridoviridae*. However, the largest number of Bcl-2 homologs are found in *poxviridae* [12] such as vaccinia and variola virus F1L [23-25] and myxomavirus M11L [26-28]. Whilst structural studies have shown [18, 21, 24, 29-31] these virus encoded Bcl-2-fold proteins there is substantial diversity with regards to which proapoptotic host Bcl-2 proteins they bind. For example, vaccinia virus F1L binds Bim, Bak and Bax only [32], whereas sheeppoxvirus SPPV14 binds Bid, Bim, Bmf, Hrk, Puma, Bak and Bax [33], and African swine fever virus A179L binds all major pro-apoptotic Bcl-2 proteins [18]. The diversity observed amongst the proapoptotic ligand binding profiles for virus encoded prosurvival Bcl-2 extends to the mechanisms of action too, for example, myxomavirus M11L primarily acts by sequestering Bak and Bax [28], whereas vaccinia virus F1L neutralizes host cell death by sequestering Bim during viral infections [23].

Tanapoxvirus encoded TPV16L is a putative homolog of deerpoxvirus DPV022 [4] (Figure 1). In order to understand the putative apoptosis regulatory function of TPV16L we examined its ability to bind to peptides of host proapoptotic Bcl-2 proteins, and determined crystal structures of TPV16L bound to its interactors. We now show that TPV16L is a highly flexible Bcl-2 fold protein that is able to bind to BH3 motif peptides of host proapoptotic Bcl-2 proteins with high affinity both as a monomeric and domain-swapped dimeric form. These findings provide a mechanistic basis for tanapox mediated inhibition of apoptosis, and highlight the substantial structural flexibility in the Bcl-2 fold that allows multiple oligomeric topologies to engage proapoptotic interactors using the canonical ligand binding groove.

Materials and methods

Protein expression and purification

Synthetic cDNA encoding for codon optimized wildtype TPV16L (Uniprot Accession number Q9DHU6) as well as three mutants TPV16L (K52A, R90A and A96I) lacking 23 C-terminal residues were cloned into the bacterial expression vector pGex-6p-1 (Genscript). Recombinant TPV16L was expressed in C41(DE3) cells in 2YT medium supplemented with 1 mg/ml ampicillin at 37°C in a shaking incubator until an OD_{600} of 0.6 was reached. The protein expression was induced by adding isopropyl β-D-1-thiogalactopyranoside (IPTG) to final concentration of 0.75 mM for 18 hours at 20°C. Bacterial cells were harvested by centrifugation at 5000 rpm (JLA 9.1000 rotor, Beckman Coulter Avanti J-E) for 20 min and re-suspended in 100 ml lysis buffer A (50 mM Tris pH 8.0, 300 mM NaCl and 10 mM DTT (dithiothreitol). The cells were homogenized using an Avestin EmulsiFlex homogenizer and lysed using sonication (programme 7, Fisher Scientific™ Model 705 Sonic Dismembrator) and the resultant lysate was transferred into SS34 tubes for further centrifugation at 18,000 rpm (JA-25.50 rotor, Beckman Coulter Avanti J-E) for 30 min. The supernatant was loaded onto 5 mL of glutathione sepharose 4B (GE Healthcare) equilibrated with buffer A. After sample application, the column was washed with 150 ml of buffer A and protein on-column cleavage was achieved by adding HRV 3C protease overnight at 4°C. The cleaved protein was eluted using buffer A, with the remaining protein being concentrated using a centrifugal concentrator with 3 kDa molecular weight cut-off (Amicon® Ultra 15) to a final volume of 2 ml. Concentrated TPV16L was subjected to size-exclusion chromatography using a Superdex S200 increase 10/300 column mounted on an ÄKTA Pure system (GE Healthcare) equilibrated in 25 mM HEPES pH 7.5, 150 mM NaCl and 5 mM TCEP (Tris(2-carboxyethyl)phosphine hydrochloride), and fractions analysed using SDS-PAGE. The final sample purity was estimated to be higher than 95% based on SDS–PAGE analysis. Appropriate fractions were pooled and concentrated using a centrifugal concentrator with 3 kDa molecular weight cut-off (Amicon ® Ultra 15) to final concentration of 5.4 mg/ml.

116

117 **Analytical ultracentrifugation**

118 Sedimentation velocity experiments were performed in a Beckman Coulter XL-A analytical
119 ultracentrifuge as described previously [34-37]. Briefly, double sector quartz cells were
120 loaded with 400 µl of buffer (25 mM HEPES pH 7.5, 150 mM NaCl, 5mM TCEP) and
121 380 µl of sample (solubilized in buffer). For the runs with apo protein, initial concentrations
122 of 0.2 mg/ml, 0.4 mg/ml and 0.8 mg/ml were employed. For the runs with the complexes, the
123 protein and peptide concentrations were kept at 0.2 mg/ml. The cells were loaded into an
124 An50-Ti rotor and the experiments conducted at 25°C. Initial scans were carried out at
125 3,000 rpm to determine the optimal wavelength and radial positions. Final scans were
126 performed at 40,000 rpm and data were collected continuously at 230 nm using a step size
127 of 0.003 cm without averaging. Solvent density, solvent viscosity and estimates of the
128 partial specific volume of apo TPV16L, TPV16L:Bim, TPV16L:Puma and TPV16L:Bax. at
129 25°C were calculated using SEDNTERP [38]. Data were fitted using the SEDFIT software
130 (www.analyticalultracentrifugation.com) to a continuous size-distribution model [39-41].

131

132 **Measurement of dissociation constants**

133 Binding affinities were measured using a MicroCal iTC200 system (GE Healthcare) at 25°C
134 using wild type TPV16L as well as three mutants TPV16L K52A, R901 and A96I in 25 mM
135 HEPES pH 7.5, 150 mM NaCl, 5 mM TCEP at a final concentration of 30 µM. BH3 motif
136 peptide ligands were used at a concentration of 300 µM and titrated using 19 injections of 2.0
137 µl of ligand. All affinity measurements were performed in triplicate. Protein concentrations
138 were measured using a Nanodrop UV spectrophotometer (Thermo Scientific) at a wavelength
139 of 280 nm. Peptide concentrations were calculated based on the dry peptide weight after
140 synthesis. The BH3-motif peptides used were commercially synthesized and were purified to

a final purity of 95% (GenScript) and based on the human sequences. Bim: DMRPEIWIAQELRRIGDEFNAYYARR (UniProt accession code O43521, residues 141-166), Puma: EEQWAREIGAQLRRMADDLNAQYERR (accession code Q9BXH1, residues 130-155), Bik: MEGSDALALRLACIGDEMDVSLRAP (accession code Q13323, residues 51-75), Bax: VPQDASTKKLSECLKRIGDELDSNMELQ (accession code Q07812, residues 50-77), Bak PSSTMGQVGRQLAIIGDDINRRYDSE (accession code Q16611, residues 67-92), Bid: QEDIIRNIARHLAQVGDSMDRSIPPG (accession code P55957, residues 79-104), Bad: NLWAAQRYGRELRRMSDEFVDSFKKG (accession code Q92934 ,residues 103-128), Bmf: GQWQHQAEVQIARKLQCIADQFHRLHVQQ (accession code Q96LC9, residues 123-151), Noxa: PAELEVECATQLRRFGDKLNFRQKLL (accession code Q13794, residues 18-43), Bok: VPGRLAEVCAVLLRLGDELEMIRPSV (accession code Q9UMX3, residues 59-84), Hrk: RSSAAQLTAARLKAIGDELHQRTMWR (accession code O00198, residues 26-51).

Crystallization and structure determination

Crystals for TPV16L: Bax BH3, TPV16L: Puma BH3 or TPV16L: Bim BH3 complexes were obtained by mixing TPV16L with human Bax BH3 28-mer or Puma BH3 26-mer peptide into 1:1.25 molar ratio as described previously [42] and concentrated using a centrifugal concentrator with 3 kDa molecular weight cut-off (Amicon ® Ultra 0.5) to 5 mg/ml and concentrated protein was immediately used for crystallization trials. Initial high throughput sparse matrix screening was performed using 96 well sitting drop trays (swissic, Neuheim, Switzerland).

TPV16L: Bax BH3 crystals were grown by the sitting drop vapour diffusion method at 20°C in 1.0 M LiCl, 0.1 M Citrate pH 4.0, 20 % W/V PEG 6000. The crystals were flash cooled at -173°C in mother liquor supplemented with 20% ethylene glycol. The TPV16L:

Bax BH3 complex formed single square bipyramidal crystals belong to space group $P4_32_12$ with a = 55.36 Å, b = 55.36 Å, c = 126.96 Å, α = 90.00 Å, β = 90.00 Å, γ = 90.00 Å in the tetragonal crystal system.

Diffraction data were collected at the Australian Synchrotron MX2 beamline using an Eiger detector with an oscillation range 0.1° per frame with a wavelength of 0.9537 Å, integrated using XDS [43] and scaled using AIMLESS [44]. Molecular replacement was carried out using PHASER [45] with the previously solved structure of DPV022 (PDB ID: 4UF1 [29]) as a search model. TPV16L: Bax BH3 crystals contained one molecule of TPV16L and one Bax BH3 peptide in the asymmetric unit, with 46.3% solvent content and final TFZ and LLG values of 8.0 and 52.79 respectively. The final model of TPV16L: Bax BH3 was built manually over several cycles using Coot [46] and refined using PHENIX [47] with final R_{work}/R_{free} of 0.23/0.25, with 99.1% of residues in the favoured region of the Ramachandran plot and no outliers.

TPV16L: Puma BH3 crystals were grown as the TPV16L: Bax BH3 crystals and were obtained in 0.1 M Potassium thiocyanate, 30% PEG 2000MME. The crystals were flash cooled at -173°C in mother liquor. The TPV16L: Bax BH3 complex formed single rod-shaped crystals belong to space group $P2_12_12_1$ with a = 54.09 Å, b = 54.87 Å, c = 60.22 Å, α = 90.00 Å, β = 90.00 Å, γ = 90.00 Å in monoclinic crystal system. Diffraction data collection, integration and scaling were performed as described above. The molecular replacement was carried out using PHASER with the previously solved structure of TPV16L: Bax BH3 as a search model. TPV16L: Puma BH3 crystals contain one molecule of TPV16L and one Puma BH3 peptide, with 46.3% solvent content and final TFZ and LLG values of 13.2 and 133.15 respectively. The final model of TPV16L: Puma BH3 was built manually over several cycles using Coot and refined using PHENIX with final R_{work}/R_{free} of 0.19/0.22 with 99.3% of residues in the Ramachandran favoured region of the plot and no outliers.

TPV16L: Bim BH3 crystals were grown similar to other two complexes as above and in 0.1 M MIB buffer pH 8.0, 25% PEG 1500. The crystals were flash cooled at -173°C in mother liquor. The TPV16L: Bim BH3 complex formed single small cubic shape crystals belong to space group $P3_22_1$ with a = 59.65 Å, b = 59.65 Å, c = 90.90 Å, α = 90.00 Å, β = 90.00 Å, γ=120.00 Å in hexagonal crystal system. Diffraction data collection, integration and scaling were performed as described above. Molecular replacement was carried out using PHASER with the previously solved structure of TPV16L: Bax BH3 as a search model. TPV16L: Bim BH3 crystals contain one molecule of TPV16L and one Bim BH3 peptide, with 44.01% solvent content and final TFZ and LLG values of 15.8 and 208.64 respectively. The final model of TPV16L: Bim BH3 was built manually and refined as described above to yield a final R_{work}/R_{free} of 0.24/0.27 with 98% of residues in Ramachandran favoured region of the plot and no outliers. Coordinate files have been deposited in the Protein Data Bank under the accession codes 6TPQ, 6TQQ and 6TRR. All images were generated using the PyMOL Molecular Graphics System, Version 1.8 Schrödinger, LLC. All software was accessed using the SBGrid suite [48]. All raw diffraction images were deposited on the SBGrid Data Bank [49] using their PDB accession code 6TPQ, 6TQQ and 6TRR.

Sequence alignment

Sequence alignments were performed using MUSCLE [50] (https://www.ebi.ac.uk/Tools/msa/muscle/) with the default settings, and sequence identities were calculated based on the total number of conserved residues in TPV16L against the full sequence.

Yeast colony assays

Saccharomyces cerevisiae W303α cells were co-transformed with pGALL(TRP) vector only, pGALL(TRP)-Bcl-x_L, or pGALL(TRP)-TPV16L and pGALL(Leu)-Bak or pGALL(Leu)-Bax. pGALL(TRP) and pGALL(Leu) places genes under the control of a galactose inducible promoter [51]. Cells were subsequently spotted as a 5-fold serial dilution series onto medium supplemented with 2% w/v galactose (inducing, "ON") to induces protein expression, or 2% w/v glucose (repressing, "OFF"), which prevents protein expression, as previously described [52]. Plates were incubated for 48 h at 30˚C and then photographed.

Results

In order to reveal the function for TPV16L, we recombinantly expressed and purified TPV16L lacking the C-terminal 23 residues and examined its ability to bind to peptides spanning the BH3 motif of all proapoptotic human Bcl-2 proteins using isothermal titration calorimetry (ITC). TPV16L bound to a number of BH3 motif peptides with high affinity, including those from the BH3-only proteins Bim, Bid, Hrk and Puma as well as those from the multimotif executor proteins Bak and Bax (Figure 2, Table 1). We then utilized a yeast based heterologous expression system for studying functional interactions of TPV16L with Bak and Bax [13]. Consistent with our ITC data, we observed that TPV16L could directly counter Bak and Bax induced yeast growth arrest when these proteins were overexpressed in yeast (Figure 3).

To understand the structural basis for proapoptotic Bcl-2 binding by TPV16L we then determined the crystal structure of TPV16L bound to the human Bax, Bim and Puma BH3 motifs (Figure 4, Table 2). In the TPV16L:Bax BH3 complex, TPV16L adopts a globular Bcl-2 fold comprising 7 α-helices (Figure 4a). Similar to vaccinia and variola virus F1L and deerpoxvirus DPV022 TPV16L adopts a domain-swapped dimeric topology where the α1 helix from one protomer is swapped with that of a second protomer in the complex, taking up

the space vacated by the matching α1 helix (Figures 4a, c). Superimposition of one chain of the TPV16L from the domain-swapped dimer TPV16L:Bax BH3 complex with the equivalent chain from the domain-swapped dimer VACV F1L from F1L:Bak BH3 [23] and the domain-swapped dimer DPV022 from DPV022:Bax BH3 [29] (Figures 4c, S2) yields an rmsd of 2.3 Å (superimposed over 122 Cα atoms) and 2.1 Å (superimposed over 131 Cα atoms), respectively, whereas superimposition of the entire domain-swapped dimer of TPV16L yields rmsd values of 2.2 and 2.7 Å, respectively. The position of the TPV16L α1 within the domain-swapped dimer is identical to VACV F1L and DPV022 (Figure S2). Similarly, TPV16L in the TPV16L:Bim BH3 complex adopts a domain swapped dimeric configuration that is identical to the TPV16L:Bax BH3 complex (Figure 4b).

Unexpectedly, TPV16L in the TPV16L: Puma BH3 complex adopts a monomeric Bcl-2 fold, where the α1 helix is folded back into the side of the globular Bcl-2 fold (Figure 4d). A DALI analysis [53] indicated that the closest homolog in the PDB is myxomavirus M11L (Figure 4e, PDB ID 2JBX [28]) with an rmsd of 2.1 Å (over 111 Cα), whereas the closest mammalian Bcl-2 structure is human Mcl-1 (PDB ID 5FC4 [54]) with an rmsd of 2.3 Å (over 126 Cα) (Figure S2c).

TPV16L utilized the canonical Bcl-2 ligand binding groove formed by α2-5 to engage BH3 motif ligands (Figure 5, S1). In the TPV16L:Bax BH3 complex (Figure 5a), Bax residues L157, L161, I164 and L168 protrude into the four hydrophobic pockets of TPV16L. In addition, ionic interactions are observed between TPV16L R90 guanidium group and Bax D166 carboxyl as well as TPV16L R90 guanidium group and Bax D169 carboxyl group, with a further three hydrogen bonds between the TPV16L S84 hydroxyl group and the Bax S158 hydroxyl group, TPV16L R90 guanidium group and Bax K162 amine as well as TPV16L S92 hydroxyl group and the main chain amide group of Bax G165 (Figure 5a).

In the TPV16L:Bim BH3 complex (Figure 5b), Bim residues I157, L161, I164 and F168 are used to engage the four hydrophobic pockets in TPV16L. Furthermore, there is one ionic interaction between TPV16L R90 guanidium group and Bim D166 carboxyl group and a hydrogen bond between TPV16L N87 amide and Bim R162 guanidium group. In the TPV16L: Puma BH3 complex (Figure 5c), Puma utilizes the four hydrophobic residues I136, L140, M143 and L147 to engage the four hydrophobic pockets in TPV16L. These hydrophobic interactions are supplemented by ionic interactions between TPV16L R90 guanidium group and Puma D145 carboxyl group as well as TPV16L K52 ammonium group and Puma D146 carboxyl group. Furthermore, two hydrogen bonds are found between TPV16L Y53 hydroxyl and Puma D146 carboxyl group, and between the TPV16L N56 sidechain amide and Puma Q139 sidechain carbonyl groups. Superimposition of monomeric TPV16L from the complex with Puma BH3 with one of the chains from the domain-swapped dimeric form of TPV16L from the Bax BH3 complex yields an rmsd of 1.2 Å over α2-7 (117 Cα atoms), indicating that despite the topology change from monomer to domain-swapped dimer the regions of TPV16L not involved in the domain swap remain near identical.

Since we observed TPV16L in both a monomeric and domain-swapped dimeric topology, we subjected TPV16L and some of its complexes with BH3 motif peptides to analytical ultracentrifugation (AUC). AUC was performed on TPV16L alone as well as on TPV16L bound to Bim, Bax and Puma BH3 (Figure 6). TPV16L alone revealed a mixture of monomeric and dimeric protein at concentrations ranging from 0.2-0.8 mg/mL, with a ratio of monomer:dimer of ~3.5:1. Similarly, complexes of TPV16L with Bim, Bax and Puma BH3 at 0.2 mg/mL also revealed a mixture of heterodimers and heterotetramers, with the ratio of TPV16L:Bim BH3 heterodimers vs heterotetramers being ~4:1, with TPV16L: Bax and Puma complexes displaying comparable ratios of ~3.5:1, respectively, closely matching the ratio observed for TPV16L alone (Figure 6).

To validate the crystal structures of TPV16L bound to Bim, Bax and Puma BH3 we performed structure-guided mutagenesis (Figure 5d) and analysed the mutants for their ability to bind to proapoptotic BH3 motif peptides (Table 1). Mutation of the conserved R90 in TPV16L substantially impacts on its ability to bind BH3 motif peptides, with 10-80 fold reduction in affinities for Bim, Bad, Bid, Bik as well as Bak and Bax BH3 binding, whereas binding to Hrk and Puma BH3 is only reduced ~2-fold. Similarly, an A96I substitution led to affinity losses of 2-40 fold across all interactors. In contrast, whilst mutation of K52 to Ala also led to a 2-4 fold reduction in binding affinities for many interactors, binding to Bid BH3 was largely unaffected. In contrast, binding to Bad and Bmf BH3 was reduced by 40 and 20 fold, respectively.

Discussion

Altruistic death of an infected cell is a potent mechanism to restrict viral infections. Viruses have evolved numerous strategies to prevent premature host cell death to establish productive infections [12]. Tanapoxvirus encodes TPV16L, a putative Bcl-2 homolog, and we now show that TPV16L adopts both a classical monomeric form as well as a domain-swapped dimer. Dimeric TPV16L is able to bind both BH3-only proteins as well as the BH3 regions of Bak and Bax. TPV16L harbours a broad proapoptotic BH3 ligand binding profile when compared to other poxvirus encoded domain-swapped pro-survival Bcl-2 proteins. The poxvirus encoded pro-survival Bcl-2 homologs VACV F1L [32], VARV F1L [24] and deerpoxvirus DPV022 [29] all have similar dimeric topologies to TPV16L dimer but feature more restricted interaction and affinity profiles. VACV F1L [32] and DPV022 [29] only bind to Bim, Bak and Bak whereas VARV F1L binds Bid, Bak and Bax [24]. In all three cases these interactions are characterized by lower affinities, in particular for Bak and Bax which bind with only micromolar affinities to VACV F1L, DPV022 F1L and DPV022. In contrast,

TPV16L displays much tighter affinities including 38 nM for Bak and 70 nM for Bax (Table 1). Intriguingly, TPV16L is able to adopt both monomeric and domain-swapped dimer topologies, however the domain swap does to not impact significantly on the configuration of the canonical ligand binding groove. Superimposition of monomeric and dimeric TPV16L reveals there are virtually no differences in the respective ligand binding grooves. However, no thermodynamic analysis has been performed to examine such effects on ligand binding.

A comparison of the overall dimeric structures of TPV16L with other domain swapped poxviral Bcl-2 dimers reveals that dimeric TPV16L superimposes on a VACV F1L dimer with an rmsd of 2.2 Å (over 266 Cα atoms) and on dimeric DPV022 with 2.7 Å (over 274 Cα atoms). This high level of similarity is achieved despite low overall sequence identity (8% between TPV16L and VACV F1L and 31% between TPV16L and DPV022). A detailed comparison of the interactions formed by TPV16L and DPV022 when bound to Bax reveals that the hallmark interaction between the conserved Asp from Bax BH3 with an Arg from TPV16L or DPV022 BH1 is preserved, as are hydrogen bonds between Bax Ser158 and Asp169 with TPV16L S84 or DPV022 E80. As expected, loss of the hallmark ionic interaction severely impacts TPV16L ability to bind to pro-apoptotic Bcl-2 interactors, with a TPV16L R90A mutation displaying up to 80 fold reduction in affinity (Table 1), as previously observed for mammalian prosurvival Bcl-2 [55]. Unlike in the DPV022 complex with Bax [29], the bulk of the BH3 peptides are engaged in the TPV16L ligand binding groove resulting in buried surface areas of 2343-3142 $Å^2$ for the complexes with Bax, Bim and Puma, whereas in DPV022:Bax BH3 only 4 helical turns are engaged that bury 2117 $Å^2$, which may contribute to the more modest affinity of the interaction. The more extensive engagement of the TPV16L binding groove with a BH3 peptide thus provides a possible rational for the substantially tighter binding observed compared with DPV022.

Virus encoded Bcl-2 proteins are not limited to domain-swapping for dimer formation (Figure S3). Vaccinia virus has been shown to encode for a suite of Bcl-2 fold proteins that modulate NF-κB signalling, which all adopt dimeric topologies utilizing an interface formed by helices α1 and 6 [56-59]. In contrast, grouper iridovirus encoded GIV66 forms dimers that occlude the canonical ligand binding groove, with binding of BH3 motif peptides dissociating the dimers [21]. Domain-swapping is not limited to virus-encoded Bcl-2 proteins, and is also observed in mammalian Bcl-2. Bcl-x_L has been shown to adopt domain-swapped topologies featuring either α5-8 or α1 swaps. However, these swaps were induced by exposure to extreme pH [60] or temperature environments [61] or by truncation of the loop connecting α1 and α2 [62], respectively. In contrast, recombinantly expressed Bcl-w lacking its C-terminal tail adopts both a monomeric state as well as a domain swapped dimeric state where α3-4 are swapped [63, 64]. Such a swap impacts the canonical ligand binding groove, and leads to differential binding affinities between monomeric and dimeric Bcl-w [64]. Domain swapping has also been shown for human proapoptotic Bak [65] and Bax [66], where the formation of an extended single helix comprising helices α5 and 6 leads to a core/latch configuration, where a core domain formed by α1-4 partners the latch domain formed by α6-8 from a second protomer. In contrast, catfish Bax features a domain swapped α9 helix [67]. This significant number of topological variances across dimeric Bcl-2 proteins underscores the inherent flexibility in this fold, and potentially enables additional layers of functionality to modulate function in addition to direct interactions.

In summary, we report the biochemical and structural analysis of tanapoxvirus 16L, which revealed a broad high affinity binding profile for mammalian pro-apoptotic Bcl-2 proteins. Furthermore, our crystal structures of TPV16L bound to Bax and Puma BH3 indicate that TPV16L displays substantial structural plasticity, being able to adopt both a classical monomeric Bcl-2 fold as well as a domain-swapped dimeric Bcl-2 fold. Overall, our

findings provide a mechanistic platform for dissecting the role of 16L for tanapoxvirus replication and infectivity.

Competing interests

The authors declare no competing financial interests in relation to the work described.

Author Contributions

Chathura D. Suraweera: Acquisition, analysis and interpretation of data; Drafting and revising the article.

Mohd Ishtiaq Anasir: Acquisition, analysis and interpretation of data.

Airah Javorsky: Acquisition, analysis and interpretation of data;

Srishti Chugh: Acquisition, analysis and interpretation of data.

Rachael E. Impey: Acquisition, analysis and interpretation of data.

Muhammad Hasan Zadeh: Acquisition, analysis and interpretation of data.

Tatiana P. Soares da Costa: Acquisition, analysis and interpretation of data; Drafting and revising the article.

Mark G. Hinds: Conception and design; Analysis and interpretation of data; Drafting and revising the article;

Marc Kvansakul: Conception and design; Acquisition of data; Analysis and interpretation of data; Drafting and revising the article.

Acknowledgements

We thank staff at the MX beamlines at the Australian Synchrotron for help with X-ray data collection. We thank the ACRF for their support of the Eiger MX detector at the Australian Synchrotron MX2 beamline and the Comprehensive Proteomics Platform at La Trobe

388 University for core instrument support. This research was funded by the Australian Research
389 Council (Fellowship FT130101349 to MK and DE190100806 to TPSC), National Health and
390 Medical Research Council of Australia (CDA fellowship 637372 and Project Grant
391 APP1007918 to MK). and La Trobe University (Scholarship to CDS, MIA, AJ and REI).

392 **Tables**

393 **Table 1:** Interactions of TPV16L with pro-apoptotic BH3 motif peptides. All affinities were
394 measured using isothermal titration calorimetry and K_D values given in nM as a mean of
395 three independent experiments with SD.

396

Peptide	WT	R90A	A96I	K52A
Bak	38 ± 4	2325 ± 261	1534 ± 67	113 ± 3
Bax	70 ± 5	2301 ± 374	691 ± 92	266 ± 11
Bok	NB	NB	NB	NB
Bad	132 ± 35	10206 ± 1570	4721 ± 320	5857 ± 732
Bid	719 ± 66	12675 ± 1257	1720 ± 152	976 ± 126
Bik	1250 ± 111	14356 ± 1370	3178 ± 300	3382 ± 85
Bim	196 ± 12	1766 ± 320	1824 ± 220	575 ± 36
Bmf	606 ±76	4894 ± 644	1927 ± 487	13520 ± 3810
Hrk	3550 ± 770	5378 ± 315	6279 ± 793	10081 ± 2710
Noxa	NB	NB	NB	NB
Puma	468 ± 47	941 ± 54	817 ± 31	1010 ± 130

397
398

Table 2: X-ray data collection and refinement statistics. Values in parentheses are for the highest resolution shell.

	TPV16L:Bax BH3	**TPV16L:Puma BH3**	**TPV16L:Puma BH3**
Data collection			
Space group	$P4_32_12$	$P2_12_12_1$	$P3_22_1$
Cell dimensions			
a, b, c (Å)	55.38, 55.38, 126.94	54.09, 54.87, 60.22	59.65, 59.65, 90.90
α, β, γ (°)	90 90 90	90, 90, 90	90, 90, 120
Wavelength (Å)	0.9537	0.9537	0.9537
Resolution (Å)	33.33-2.12 (2.19-2.12)	32.45-1.85 (1.91-1.85)	44.92-3.00 (3.11-3.00)
R_{sym} or R_{merge}	0.097 (2.67)	0.066 (1.55)	0.168(1.50)
I / σI	11.2 (0.8)	11.1 (0.9)	4.3 (0.7)
Completeness (%)	99.86 (99.65)	99.51 (97.62)	99.9 (100)
$CC_{1/2}$	0.99 (0.29)	0.99 (0.40)	0.99 (0.34)
Redundancy	8.6 (6.6)	5.5 (4.7)	4.7 (4.6)
Refinement			
No. reflections	11838	15799	7992
R_{work} / R_{free}	0.239/254	0.195/0.223	0.242/0.276
Clashscore	0	2.17	2.66
No. atoms			
Protein	1291	1369	1298
Ligand/ion	2	1	1
Water	23	91	8
B-factors			
Protein	65.68	51.74	72.84
Ligand/ion	84.20	86.29	63.59
Water	60.76	50.89	65.12
R.m.s. deviations			
Bond lengths (Å)	0.003	0.006	0.003
Bond angles (°)	0.44	0.67	0.51

Figure legends

Figure 1: Sequence alignment of TPV16L with pro-survival Bcl-2 family members. The sequences of tanapoxvirus 16L (uniprot accession number: A7XCC0), deerpoxvirus DPV022 (uniprot accession number: Q08FX8), vaccinia virus F1L (uniprot accession number: O57173), myxomavirus M11L (uniprot accession number: Q85295) and human Bcl-x_L (uniprot accession number: Q07817) were aligned using MUSCLE [50]. Secondary structure elements are marked based on the crystal structure of TPV16L, and BH motifs are boxed and shown in bold [68]. The regions of helix are marked 'H' and unstructured loops with a bar above the sequence, conserved residues are denoted by '*', with highly conservative substitutions indicated by ':' and conserved substitutions indicated by '.'.

Figure 2: TPV16L engages a broad spectrum of BH3 motif peptides of pro-apoptotic Bcl-2 proteins. The affinities of recombinant TPV16L for BH3 motif peptides (26-mers, except for a Bid 34-mer and Bax 28-mers) were measured using ITC and the raw thermograms shown. K_D values (in nM) are the means of 3 experiments ± SD NB: no binding detected. The binding affinities are tabulated in Table 1.

Figure 3: TPV16L is able to prevent Bak and Bax induced yeast growth arrest. Yeast co-transformed with constructs encoding Bax or Bak and the indicated pro-survival proteins, each under the control of an inducible (GAL) promoter, were spotted onto inducing galactose ("ON") or repressing glucose ("OFF") plates as 5-fold serial dilutions. Images are representative of 2 independent experiments.

Figure 4: Crystal structures of TPV16L bound to Bax, Puma and Bim BH3 motifs.

(**a**) TPV16L (slate) in complex with the Bax BH3 domain (yellow). TPV16L helices are

429 labelled α1-7. The left-hand view is of the hydrophobic binding groove of one protomer
430 formed by helices α3-5, the right-hand view is the domain swapped dimer viewed along the
431 2-fold symmetry axis between the domain-swapped α1 helices. (**b**) TPV16L (slate) in
432 complex with the Bim BH3 domain (dark green) (**c**) DPV022 (cyan) in complex with the Bax
433 BH3 domain (yellow) [29]. The view is as in (a). (**d**) TPV16L (slate) in complex with the
434 Puma BH3 domain (olive) **(e)** Myxoma virus M11L (green) in complex with Bak BH3
435 (magenta). All structures were aligned using DALI pairwise alignment [53] and the view is as
436 in (a). The view in the right-hand panels in (b) and (c) are as in (a).
437
438 **Figure 5:** Detailed view of the TPV16L: Bax, Bim and Puma BH3 interfaces and mutation
439 sites. **a**) Surface depiction of the TPV16L: Bax BH3 complex. The TPV16L surface,
440 backbone and floor of the binding groove are shown in grey and pink respectively, while Bax
441 BH3 is shown as a yellow ribbon. The four key hydrophobic residues of Bax BH3 (L157,
442 L161, I164 and 168L) are protruding into the binding groove, and the conserved salt-bridge
443 formed by Bax D166 and TPV16L R90 are labeled, as well as residues involved in hydrogen
444 bonds. **b**) TPV16L:Bim BH3 with the surface of TPV16L is shown as in (a), and Bim BH3
445 is shown in dark green. The four key hydrophobic residues of Bim BH3 (I157, L161, I164
446 and F168) are protruding into the binding groove, and the conserved salt-bridge formed by
447 Bim D166 and TPV16L R90 are labeled, as well as residues involved in hydrogen bonds.
448 Interactions are denoted as black dotted lines. **c**) TPV16L:Puma BH3 is shown as in (a), with
449 Puma BH3 shown in olive. The four key hydrophobic residues of Puma BH3 (I136, L140,
450 M143 and L147) are protruding into the binding groove, and the conserved salt-bridge
451 formed by Puma D145 and TPV16L R90 are labeled, as well as residues involved in
452 hydrogen bonds. Interactions are denoted as black dotted lines. **d)** TPV16L is shown as a
453 grey surface, with locations of mutations used to investigate the binding site shaded in red.

The views were selected for the clearest view of the groove interactions in each case.

Figure 6: Sedimentation velocity analytical ultracentrifugation analysis of **a,b)** TPV16L on its own at initial concentrations of 0.2 mg/ml (black), 0.4 mg/ml (orange) and 0.8 mg/ml (purple) and **c,d)** TPV16L at an initial concentration of 0.2 mg/ml unliganded (black) and in complex with Bim (blue), Bax (green) or Puma (red). *Top panels* – Residuals resulting from the sedimentation coefficient distribution *c(s)* **(a,c)** and distribution of molar masses *c(M)* **(b,d)** best fits are plotted as a function of radial position. The residuals for the given curves are shown in the same colour above the plots. M denotes monomeric, D dimeric and T tetrameric species.

Supplementary figure legends

Figure S1: 2Fo-Fc electron density maps of **(a)** TPV16L:Bax BH3 complex interface. **(b)** TPV16L:Puma BH3 complex interface. **(c)** TPV16L:Bim BH3 complex interface. All maps were contoured at 1.5 σ. The N- and C-termini of the BH3 peptides are labelled and the structures aligned as in Figure 4. The view was selected for observational clarity of the BH3 peptide side chains.

Figure S2: Superimposition of TPV16L complexes with other closely related Bcl-2 proteins. **(a)** Superimposition of the Cα backbone of TPV16L:Bax BH3 (slate and yellow) with DPV022:Bax BH3 (cyan and yellow, PDB ID 4UF2). **(b)** TPV16L:Bax BH3 (slate and yellow) with DPV022:Bak BH3 (cyan and magenta, PDB ID 4UF1) **(c)** TPV16L:Puma BH3 (slate and green) (green) with human Mcl-1:Puma BH3 (raspberry and green, PDB ID 6QFM), the most similar structure to that of TPV16L:Puma BH3 identified using Dali. All

479 views are into the canonical ligand binding groove formed by helices α2-5. Superimpositions
480 were generated using pairwise Dali alignment [53].
481
482 **Figure S3:** Cartoon diagrams of dimeric topologies in the Bcl-2 family **(a)** Vaccinia virus
483 N1L homodimer (cyan, PDB ID 2UXE) [59]. **(b)** Grouper iridovirus GIV66 (green, PDB ID
484 5VMN) [21]. **(c)** Human Bcl-w (sand, PDB ID 2Y6W) [64]. **(d)** Human Bcl-x_L (red, PDB ID
485 1R2D) [60]. **(e)** Human Bak core-latch dimer (magenta, PDB ID 4U2U) [65]. **(f)** Human Bax
486 core-latch dimer (blue, PDB ID 4ZIE) [66]. **(g)** Catfish Bax groove-tail dimer (yellow and
487 orange, PDB ID 5W63) [67].
488

References:

1. Downie, A. W., Taylor-Robinson, C. H., Caunt, A. E., Nelson, G. S., Manson-Bahr, P. E. & Matthews, T. C. (1971) Tanapox: a new disease caused by a pox virus, *Br Med J.* **1**, 363-8.
2. Knight, J. C., Novembre, F. J., Brown, D. R., Goldsmith, C. S. & Esposito, J. J. (1989) Studies on Tanapox virus, *Virology.* **172**, 116-24.
3. Brunetti, C. R., Paulose-Murphy, M., Singh, R., Qin, J., Barrett, J. W., Tardivel, A., Schneider, P., Essani, K. & McFadden, G. (2003) A secreted high-affinity inhibitor of human TNF from Tanapox virus, *Proc Natl Acad Sci U S A.* **100**, 4831-6.
4. Nazarian, S. H., Barrett, J. W., Frace, A. M., Olsen-Rasmussen, M., Khristova, M., Shaban, M., Neering, S., Li, Y., Damon, I. K., Esposito, J. J., Essani, K. & McFadden, G. (2007) Comparative genetic analysis of genomic DNA sequences of two human isolates of Tanapox virus, *Virus Res.* **129**, 11-25.
5. Kvansakul, M. & Hinds, M. G. (2015) The Bcl-2 family: structures, interactions and targets for drug discovery, *Apoptosis.* **20**, 136-50.
6. Banjara, S. S., C.D.; Hinds, M.G.; Kvansakul, M. (2020) The Bcl-2 Family: Ancient Origins, Conserved Structures, and Divergent Mechanisms., *Biomolecules.* **10**, 128.
7. Kvansakul, M. & Hinds, M. G. (2013) Structural biology of the Bcl-2 family and its mimicry by viral proteins, *Cell Death Dis.* **4**, e909.
8. Kvansakul, M. & Hinds, M. G. (2014) The structural biology of BH3-only proteins, *Methods Enzymol.* **544**, 49-74.
9. Shamas-Din, A., Kale, J., Leber, B. & Andrews, D. W. (2013) Mechanisms of action of bcl-2 family proteins, *Cold Spring Harb Perspect Biol.* **5**, a008714.
10. McArthur, K., Whitehead, L. W., Heddleston, J. M., Li, L., Padman, B. S., Oorschot, V., Geoghegan, N. D., Chappaz, S., Davidson, S., San Chin, H., Lane, R. M., Dramicanin, M., Saunders, T. L., Sugiana, C., Lessene, R., Osellame, L. D., Chew, T. L., Dewson, G., Lazarou, M., Ramm, G., Lessene, G., Ryan, M. T., Rogers, K. L., van Delft, M. F. & Kile, B. T. (2018) BAK/BAX macropores facilitate mitochondrial herniation and mtDNA efflux during apoptosis, *Science.* **359**.
11. Tait, S. W. & Green, D. R. (2010) Mitochondria and cell death: outer membrane permeabilization and beyond, *Nat Rev Mol Cell Biol.* **11**, 621-32.
12. Kvansakul, M., Caria, S. & Hinds, M. G. (2017) The Bcl-2 Family in Host-Virus Interactions, *Viruses.* **9**, 290.
13. Kvansakul, M., Wei, A. H., Fletcher, J. I., Willis, S. N., Chen, L., Roberts, A. W., Huang, D. C. & Colman, P. M. (2010) Structural basis for apoptosis inhibition by Epstein-Barr virus BHRF1, *PLoS Pathog.* **6**, e1001236.
14. Henderson, S., Huen, D., Rowe, M., Dawson, C., Johnson, G. & Rickinson, A. (1993) Epstein-Barr virus-coded BHRF1 protein, a viral homologue of Bcl-2, protects human B cells from programmed cell death, *Proc Natl Acad Sci U S A.* **90**, 8479-83.
15. Huang, Q., Petros, A. M., Virgin, H. W., Fesik, S. W. & Olejniczak, E. T. (2002) Solution structure of a Bcl-2 homolog from Kaposi sarcoma virus, *Proc Natl Acad Sci U S A.* **99**, 3428-33.
16. Sarid, R., Sato, T., Bohenzky, R. A., Russo, J. J. & Chang, Y. (1997) Kaposi's sarcoma-associated herpesvirus encodes a functional bcl-2 homologue, *Nat Med.* **3**, 293-8.
17. Cheng, E. H., Nicholas, J., Bellows, D. S., Hayward, G. S., Guo, H. G., Reitz, M. S. & Hardwick, J. M. (1997) A Bcl-2 homolog encoded by Kaposi sarcoma-associated virus, human herpesvirus 8, inhibits apoptosis but does not heterodimerize with Bax or Bak, *Proc Natl Acad Sci U S A.* **94**, 690-4.
18. Banjara, S., Caria, S., Dixon, L. K., Hinds, M. G. & Kvansakul, M. (2017) Structural Insight into African Swine Fever Virus A179L-Mediated Inhibition of Apoptosis, *J Virol.* **91**, e02228-16.

19. Brun, A., Rivas, C., Esteban, M., Escribano, J. M. & Alonso, C. (1996) African swine fever virus gene A179L, a viral homologue of bcl-2, protects cells from programmed cell death, *Virology.* **225**, 227-30.
20. Banjara, S., Shimmon, G. L., Dixon, L. K., Netherton, C. L., Hinds, M. G. & Kvansakul, M. (2019) Crystal Structure of African Swine Fever Virus A179L with the Autophagy Regulator Beclin, *Viruses.* **11**, 789.
21. Banjara, S., Mao, J., Ryan, T. M., Caria, S. & Kvansakul, M. (2018) Grouper iridovirus GIV66 is a Bcl-2 protein that inhibits apoptosis by exclusively sequestering Bim, *J Biol Chem.* **293**, 5464-5477.
22. Lin, P. W., Huang, Y. J., John, J. A., Chang, Y. N., Yuan, C. H., Chen, W. Y., Yeh, C. H., Shen, S. T., Lin, F. P., Tsui, W. H. & Chang, C. Y. (2008) Iridovirus Bcl-2 protein inhibits apoptosis in the early stage of viral infection, *Apoptosis.* **13**, 165-76.
23. Campbell, S., Thibault, J., Mehta, N., Colman, P. M., Barry, M. & Kvansakul, M. (2014) Structural insight into BH3 domain binding of vaccinia virus antiapoptotic F1L, *J Virol.* **88**, 8667-77.
24. Marshall, B., Puthalakath, H., Caria, S., Chugh, S., Doerflinger, M., Colman, P. M. & Kvansakul, M. (2015) Variola virus F1L is a Bcl-2-like protein that unlike its vaccinia virus counterpart inhibits apoptosis independent of Bim, *Cell Death Dis.* **6**, e1680.
25. Wasilenko, S. T., Stewart, T. L., Meyers, A. F. & Barry, M. (2003) Vaccinia virus encodes a previously uncharacterized mitochondrial-associated inhibitor of apoptosis, *Proc Natl Acad Sci U S A.* **100**, 14345-50.
26. Opgenorth, A., Graham, K., Nation, N., Strayer, D. & McFadden, G. (1992) Deletion analysis of two tandemly arranged virulence genes in myxoma virus, M11L and myxoma growth factor, *J Virol.* **66**, 4720-31.
27. Douglas, A. E., Corbett, K. D., Berger, J. M., McFadden, G. & Handel, T. M. (2007) Structure of M11L: A myxoma virus structural homolog of the apoptosis inhibitor, Bcl-2, *Protein Sci.* **16**, 695-703.
28. Kvansakul, M., van Delft, M. F., Lee, E. F., Gulbis, J. M., Fairlie, W. D., Huang, D. C. & Colman, P. M. (2007) A structural viral mimic of prosurvival Bcl-2: a pivotal role for sequestering proapoptotic Bax and Bak, *Mol Cell.* **25**, 933-42.
29. Burton, D. R., Caria, S., Marshall, B., Barry, M. & Kvansakul, M. (2015) Structural basis of Deerpox virus-mediated inhibition of apoptosis, *Acta Crystallogr D Biol Crystallogr.* **71**, 1593-603.
30. Anasir, M. I., Baxter, A. A., Poon, I. K. H., Hulett, M. D. & Kvansakul, M. (2017) Structural and Functional Insight into Canarypox Virus CNP058 Mediated Regulation of Apoptosis, *Viruses.* **9**, 305.
31. Anasir, M. I., Caria, S., Skinner, M. A. & Kvansakul, M. (2017) Structural basis of apoptosis inhibition by the fowlpox virus protein FPV039, *J Biol Chem.* **292**, 9010-9021.
32. Kvansakul, M., Yang, H., Fairlie, W. D., Czabotar, P. E., Fischer, S. F., Perugini, M. A., Huang, D. C. & Colman, P. M. (2008) Vaccinia virus anti-apoptotic F1L is a novel Bcl-2-like domain-swapped dimer that binds a highly selective subset of BH3-containing death ligands, *Cell Death Differ.* **15**, 1564-71.
33. Okamoto, T., Campbell, S., Mehta, N., Thibault, J., Colman, P. M., Barry, M., Huang, D. C. & Kvansakul, M. (2012) Sheeppox virus SPPV14 encodes a Bcl-2-like cell death inhibitor that counters a distinct set of mammalian proapoptotic proteins, *J Virol.* **86**, 11501-11.
34. Soares da Costa, T. P., Yap, M. Y., Perugini, M. A., Wallace, J. C., Abell, A. D., Wilce, M. C., Polyak, S. W. & Booker, G. W. (2014) Dual roles of F123 in protein homodimerization and inhibitor binding to biotin protein ligase from Staphylococcus aureus, *Mol Microbiol.* **91**, 110-20.

588 35. Soares da Costa, T. P., Patel, M., Desbois, S., Gupta, R., Faou, P. & Perugini, M. A.
589 (2017) Identification of a dimeric KDG aldolase from Agrobacterium tumefaciens, *Proteins.*
590 **85**, 2058-2065.
591 36. Soares da Costa, T. P., Desbois, S., Dogovski, C., Gorman, M. A., Ketaren, N. E.,
592 Paxman, J. J., Siddiqui, T., Zammit, L. M., Abbott, B. M., Robins-Browne, R. M., Parker, M.
593 W., Jameson, G. B., Hall, N. E., Panjikar, S. & Perugini, M. A. (2016) Structural
594 Determinants Defining the Allosteric Inhibition of an Essential Antibiotic Target, *Structure.*
595 **24**, 1282-1291.
596 37. Soares da Costa, T. P., Christensen, J. B., Desbois, S., Gordon, S. E., Gupta, R., Hogan,
597 C. J., Nelson, T. G., Downton, M. T., Gardhi, C. K., Abbott, B. M., Wagner, J., Panjikar, S.
598 & Perugini, M. A. (2015) Quaternary Structure Analyses of an Essential Oligomeric Enzyme,
599 *Methods Enzymol.* **562**, 205-23.
600 38. Laue, T. M. (1992) Computer-aided interpretation of analytical sedimentation data for
601 proteins, *Analytical Ultracentrifugation in Biochemistry and Polymer Science*, 90-125.
602 39. Schuck, P., Perugini, M. A., Gonzales, N. R., Howlett, G. J. & Schubert, D. (2002) Size-
603 distribution analysis of proteins by analytical ultracentrifugation: strategies and application to
604 model systems, *Biophys J.* **82**, 1096-111.
605 40. Schuck, P. (2000) Size-distribution analysis of macromolecules by sedimentation
606 velocity ultracentrifugation and lamm equation modeling, *Biophys J.* **78**, 1606-19.
607 41. Perugini, M. A., Schuck, P. & Howlett, G. J. (2002) Differences in the binding capacity
608 of human apolipoprotein E3 and E4 to size-fractionated lipid emulsions, *Eur J Biochem.* **269**,
609 5939-49.
610 42. Kvansakul, M. & Czabotar, P. E. (2016) Preparing Samples for Crystallization of Bcl-2
611 Family Complexes, *Methods Mol Biol.* **1419**, 213-29.
612 43. Kabsch, W. (2010) Xds, *Acta Crystallogr D Biol Crystallogr.* **66**, 125-32.
613 44. Evans, P. (2006) Scaling and assessment of data quality, *Acta Crystallogr D Biol*
614 *Crystallogr*. **62**, 72-82.
615 45. McCoy, A. J. (2007) Solving structures of protein complexes by molecular replacement
616 with Phaser, *Acta Crystallogr D Biol Crystallogr.* **63**, 32-41.
617 46. Emsley, P., Lohkamp, B., Scott, W. G. & Cowtan, K. (2010) Features and development
618 of Coot, *Acta Crystallogr D Biol Crystallogr.* **66**, 486-501.
619 47. Echols, N., Grosse-Kunstleve, R. W., Afonine, P. V., Bunkoczi, G., Chen, V. B., Headd,
620 J. J., McCoy, A. J., Moriarty, N. W., Read, R. J., Richardson, D. C., Richardson, J. S.,
621 Terwilliger, T. C. & Adams, P. D. (2012) Graphical tools for macromolecular
622 crystallography in PHENIX, *J Appl Crystallogr.* **45**, 581-586.
623 48. Morin, A., Eisenbraun, B., Key, J., Sanschagrin, P. C., Timony, M. A., Ottaviano, M. &
624 Sliz, P. (2013) Collaboration gets the most out of software, *Elife.* **2**, e01456.
625 49. Meyer, P. A., Socias, S., Key, J., Ransey, E., Tjon, E. C., Buschiazzo, A., Lei, M., Botka,
626 C., Withrow, J., Neau, D., Rajashankar, K., Anderson, K. S., Baxter, R. H., Blacklow, S. C.,
627 Boggon, T. J., Bonvin, A. M., Borek, D., Brett, T. J., Caflisch, A., Chang, C. I., Chazin, W.
628 J., Corbett, K. D., Cosgrove, M. S., Crosson, S., Dhe-Paganon, S., Di Cera, E., Drennan, C.
629 L., Eck, M. J., Eichman, B. F., Fan, Q. R., Ferre-D'Amare, A. R., Fromme, J. C., Garcia, K.
630 C., Gaudet, R., Gong, P., Harrison, S. C., Heldwein, E. E., Jia, Z., Keenan, R. J., Kruse, A.
631 C., Kvansakul, M., McLellan, J. S., Modis, Y., Nam, Y., Otwinowski, Z., Pai, E. F., Pereira,
632 P. J., Petosa, C., Raman, C. S., Rapoport, T. A., Roll-Mecak, A., Rosen, M. K., Rudenko, G.,
633 Schlessinger, J., Schwartz, T. U., Shamoo, Y., Sondermann, H., Tao, Y. J., Tolia, N. H.,
634 Tsodikov, O. V., Westover, K. D., Wu, H., Foster, I., Fraser, J. S., Maia, F. R., Gonen, T.,
635 Kirchhausen, T., Diederichs, K., Crosas, M. & Sliz, P. (2016) Data publication with the
636 structural biology data grid supports live analysis, *Nat Commun.* **7**, 10882.

637 50. Edgar, R. C. (2004) MUSCLE: multiple sequence alignment with high accuracy and high
638 throughput, *Nucleic Acids Res.* **32**, 1792-7.
639 51. Hawkins, C. J., Wang, S. L. & Hay, B. A. (1999) A cloning method to identify caspases
640 and their regulators in yeast: identification of Drosophila IAP1 as an inhibitor of the
641 Drosophila caspase DCP-1, *Proc Natl Acad Sci U S A.* **96**, 2885-90.
642 52. Jabbour, A. M., Puryer, M. A., Yu, J. Y., Lithgow, T., Riffkin, C. D., Ashley, D. M.,
643 Vaux, D. L., Ekert, P. G. & Hawkins, C. J. (2006) Human Bcl-2 cannot directly inhibit the
644 Caenorhabditis elegans Apaf-1 homologue CED-4, but can interact with EGL-1, *J Cell Sci.*
645 **119**, 2572-82.
646 53. Holm, L. & Rosenstrom, P. (2010) Dali server: conservation mapping in 3D, *Nucleic*
647 *Acids Res.* **38**, W545-9.
648 54. Pelz, N. F., Bian, Z., Zhao, B., Shaw, S., Tarr, J. C., Belmar, J., Gregg, C., Camper, D.
649 V., Goodwin, C. M., Arnold, A. L., Sensintaffar, J. L., Friberg, A., Rossanese, O. W., Lee,
650 T., Olejniczak, E. T. & Fesik, S. W. (2016) Discovery of 2-Indole-acylsulfonamide Myeloid
651 Cell Leukemia 1 (Mcl-1) Inhibitors Using Fragment-Based Methods, *J Med Chem.* **59**, 2054-
652 66.
653 55. Sattler, M., Liang, H., Nettesheim, D., Meadows, R. P., Harlan, J. E., Eberstadt, M.,
654 Yoon, H. S., Shuker, S. B., Chang, B. S., Minn, A. J., Thompson, C. B. & Fesik, S. W.
655 (1997) Structure of Bcl-xL-Bak peptide complex: recognition between regulators of
656 apoptosis, *Science.* **275**, 983-6.
657 56. Neidel, S., Maluquer de Motes, C., Mansur, D. S., Strnadova, P., Smith, G. L. &
658 Graham, S. C. (2015) Vaccinia virus protein A49 is an unexpected member of the B-cell
659 Lymphoma (Bcl)-2 protein family, *J Biol Chem.* **290**, 5991-6002.
660 57. de Motes, C. M., Cooray, S., Ren, H., Almeida, G. M. F., McGourty, K., Bahar, M. W.,
661 Stuart, D. I., Grimes, J. M., Graham, S. C. & Smith, G. L. (2011) Inhibition of Apoptosis and
662 NF-kB Activation by Vaccinia Protein N1 Occur via Distinct Binding Surfaces and Make
663 Different Contributions to Virulence, *PLoS Pathog.* **7**, e1002430.
664 58. Graham, S. C., Bahar, M. W., Cooray, S., Chen, R. A., Whalen, D. M., Abrescia, N. G.,
665 Alderton, D., Owens, R. J., Stuart, D. I., Smith, G. L. & Grimes, J. M. (2008) Vaccinia virus
666 proteins A52 and B14 Share a Bcl-2-like fold but have evolved to inhibit NF-kappaB rather
667 than apoptosis, *PLoS Pathog.* **4**, e1000128.
668 59. Cooray, S., Bahar, M. W., Abrescia, N. G., McVey, C. E., Bartlett, N. W., Chen, R. A.,
669 Stuart, D. I., Grimes, J. M. & Smith, G. L. (2007) Functional and structural studies of the
670 vaccinia virus virulence factor N1 reveal a Bcl-2-like anti-apoptotic protein, *J Gen Virol.* **88**,
671 1656-66.
672 60. O'Neill, J. W., Manion, M. K., Maguire, B. & Hockenbery, D. M. (2006) BCL-XL
673 dimerization by three-dimensional domain swapping, *J Mol Biol.* **356**, 367-81.
674 61. Denisov, A. Y., Sprules, T., Fraser, J., Kozlov, G. & Gehring, K. (2007) Heat-induced
675 dimerization of BCL-xL through alpha-helix swapping, *Biochemistry.* **46**, 734-40.
676 62. Oberstein, A., Jeffrey, P. D. & Shi, Y. (2007) Crystal structure of the Bcl-XL-Beclin 1
677 peptide complex: Beclin 1 is a novel BH3-only protein, *J Biol Chem.* **282**, 13123-32.
678 63. Hinds, M. G., Lackmann, M., Skea, G. L., Harrison, P. J., Huang, D. C. & Day, C. L.
679 (2003) The structure of Bcl-w reveals a role for the C-terminal residues in modulating
680 biological activity, *EMBO J.* **22**, 1497-507.
681 64. Lee, E. F., Dewson, G., Smith, B. J., Evangelista, M., Pettikiriarachchi, A., Dogovski, C.,
682 Perugini, M. A., Colman, P. M. & Fairlie, W. D. (2011) Crystal Structure of a BCL-W
683 Domain-Swapped Dimer: Implications for the Function of BCL-2 Family Proteins, *Structure.*
684 **19**, 1467-76.
685 65. Brouwer, J. M., Westphal, D., Dewson, G., Robin, A. Y., Uren, R. T., Bartolo, R.,
686 Thompson, G. V., Colman, P. M., Kluck, R. M. & Czabotar, P. E. (2014) Bak core and latch

687 domains separate during activation, and freed core domains form symmetric homodimers,
688 *Mol Cell*. **55**, 938-946.
689 66. Czabotar, P. E., Westphal, D., Dewson, G., Ma, S., Hockings, C., Fairlie, W. D., Lee, E.
690 F., Yao, S., Robin, A. Y., Smith, B. J., Huang, D. C., Kluck, R. M., Adams, J. M. & Colman,
691 P. M. (2013) Bax crystal structures reveal how BH3 domains activate Bax and nucleate its
692 oligomerization to induce apoptosis, *Cell*. **152**, 519-31.
693 67. Robin, A. Y., Iyer, S., Birkinshaw, R. W., Sandow, J., Wardak, A., Luo, C. S., Shi, M.,
694 Webb, A. I., Czabotar, P. E., Kluck, R. M. & Colman, P. M. (2018) Ensemble Properties of
695 Bax Determine Its Function, *Structure*. **26**, 1346-1359 e5.
696 68. Petros, A. M., Olejniczak, E. T. & Fesik, S. W. (2004) Structural biology of the Bcl-2
697 family of proteins, *Biochim Biophys Acta*. **1644**, 83-94.
698

Figure 1

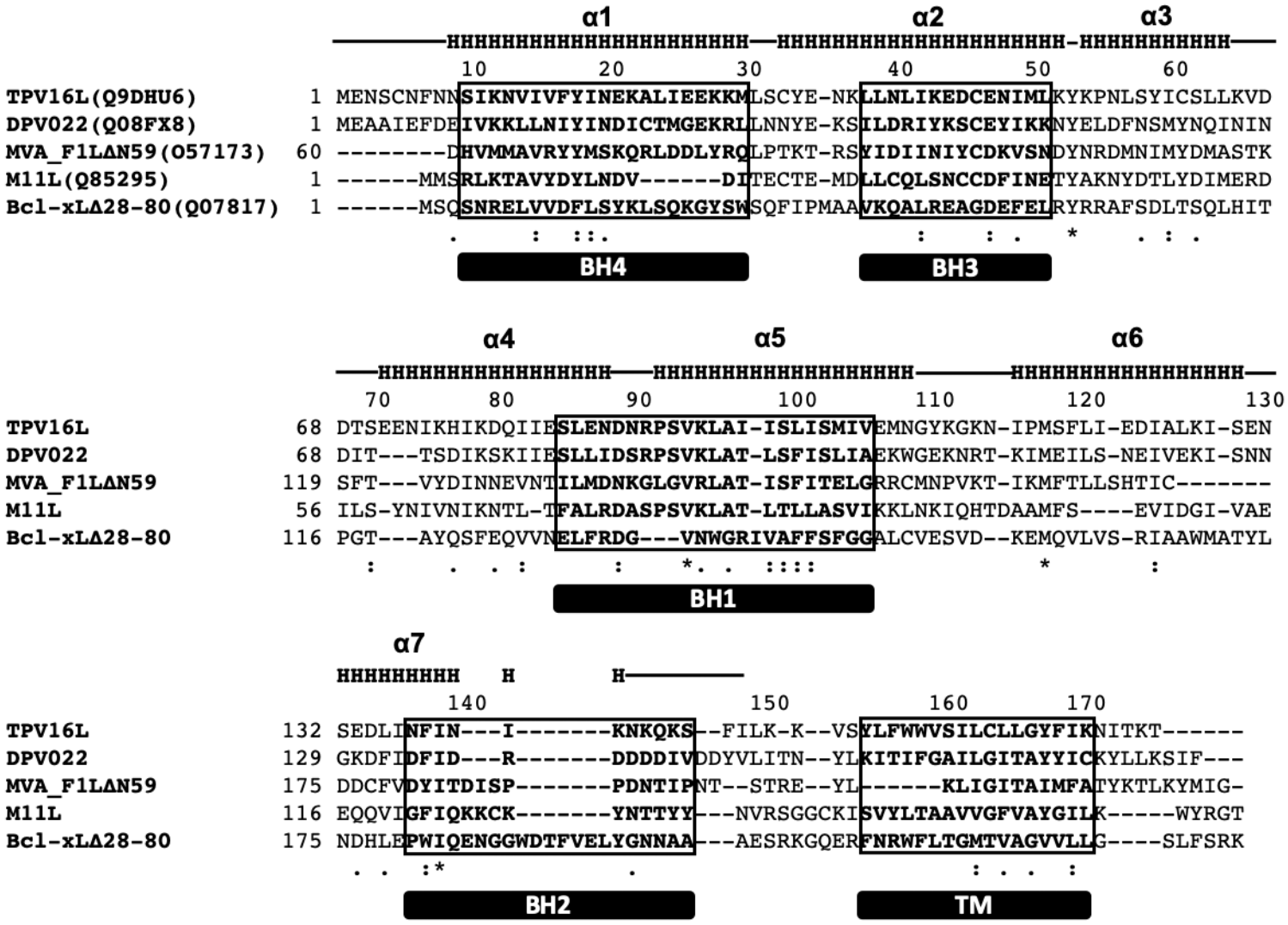

Figure 2

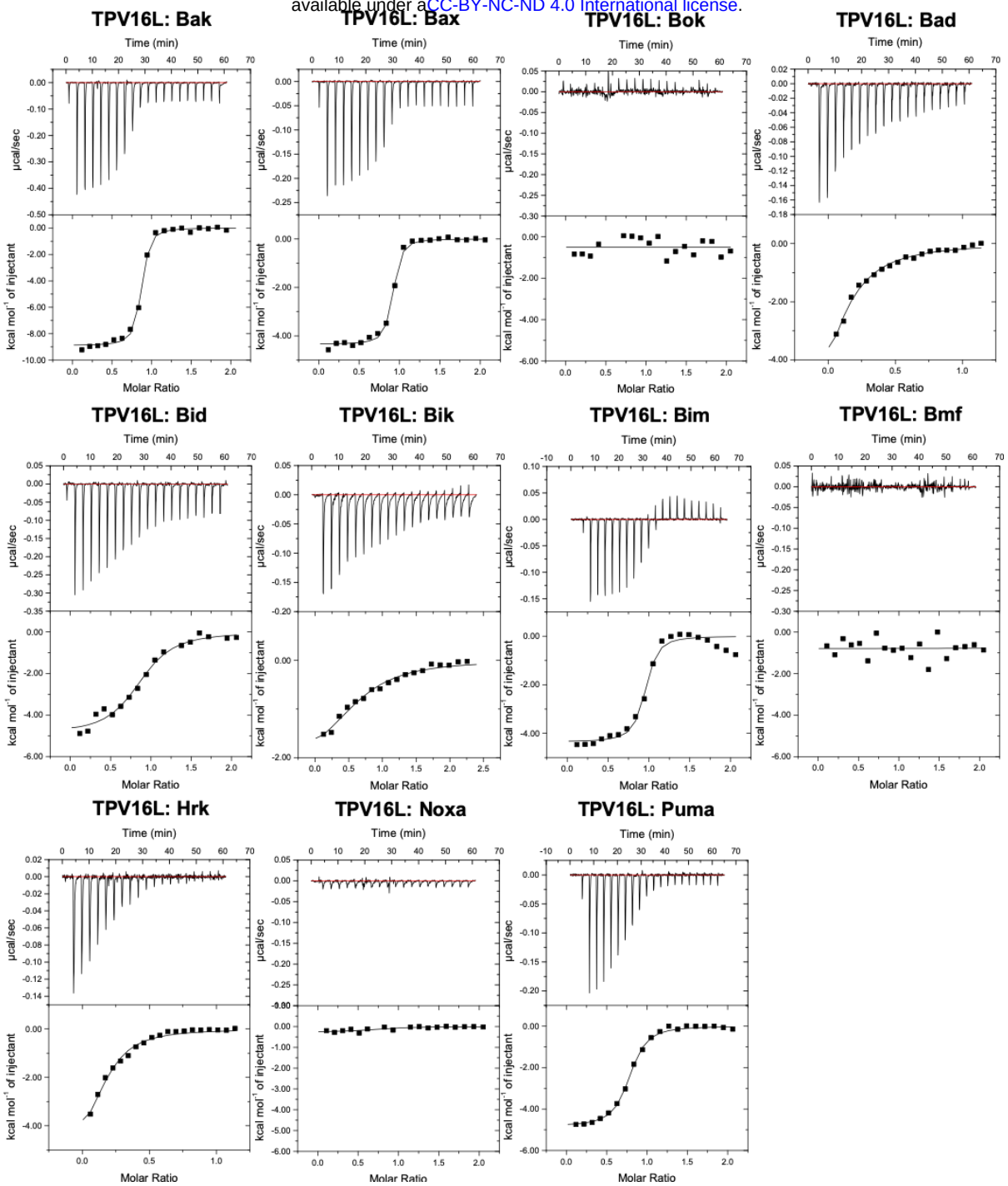

Figure 3

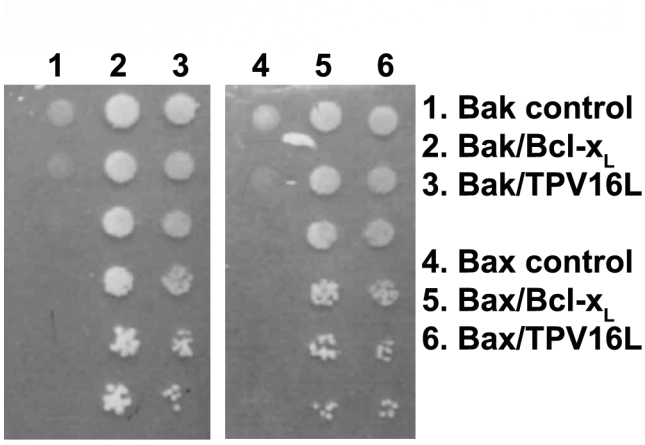

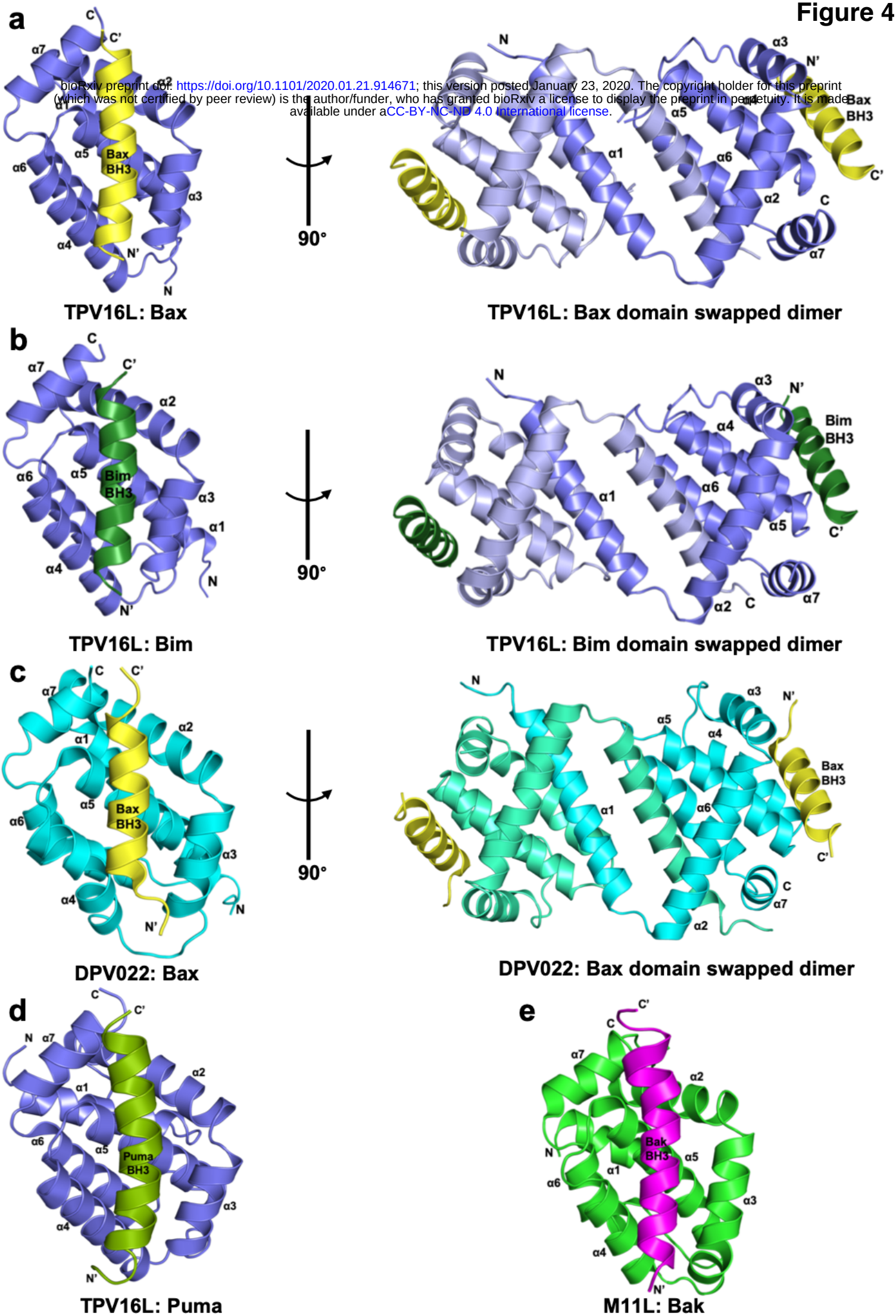

Figure 5

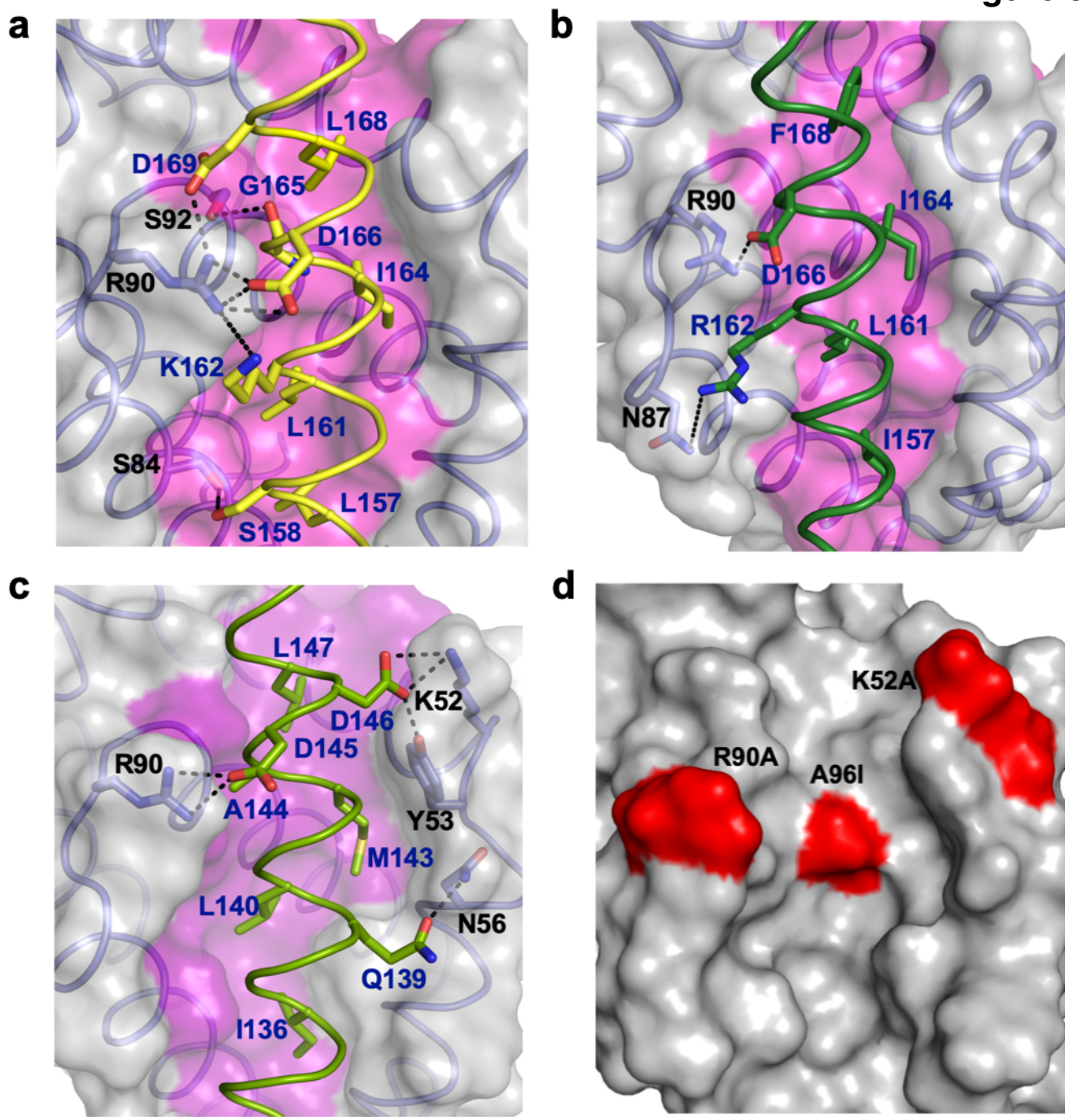

Figure 6

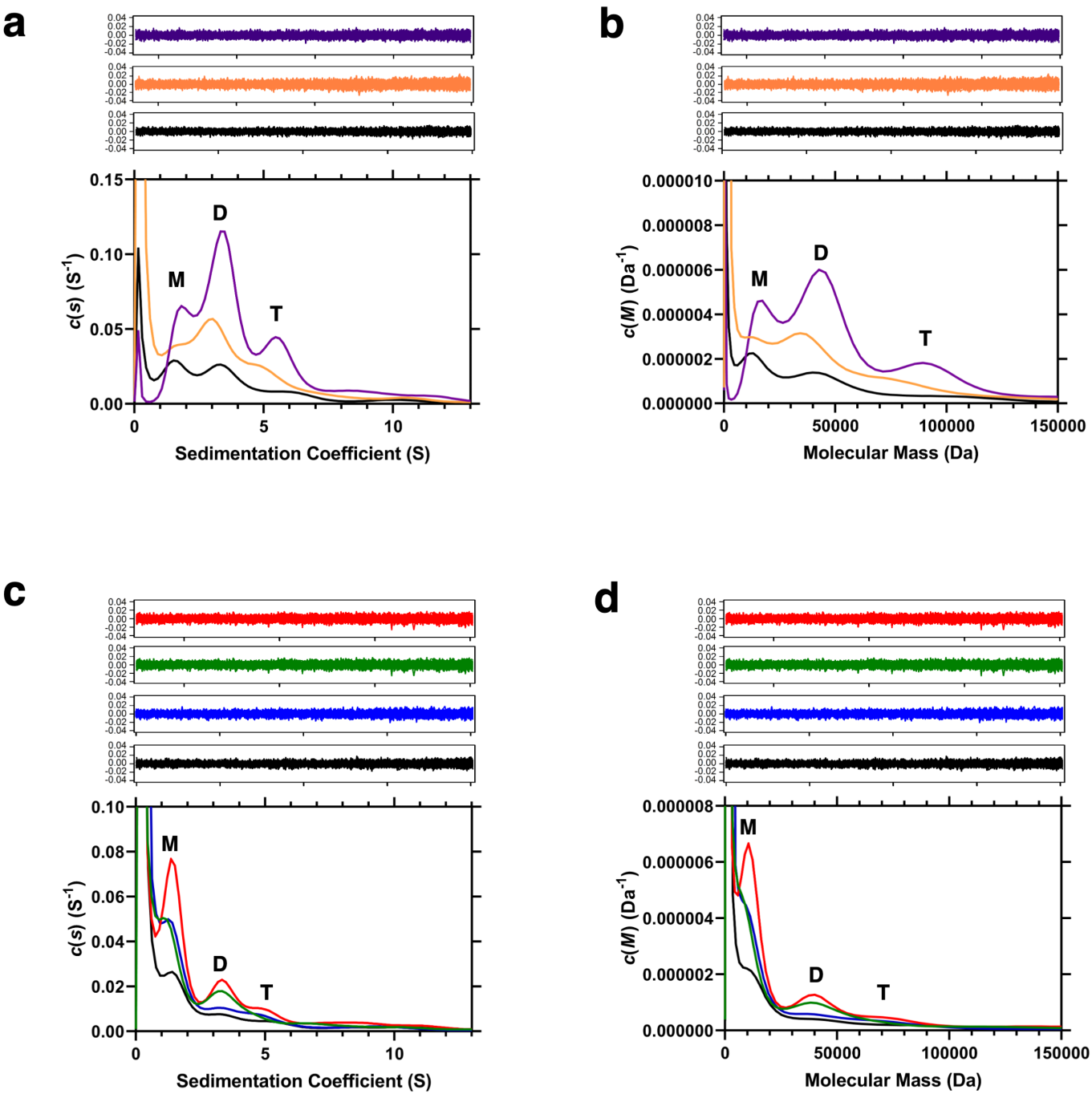

Figure S1

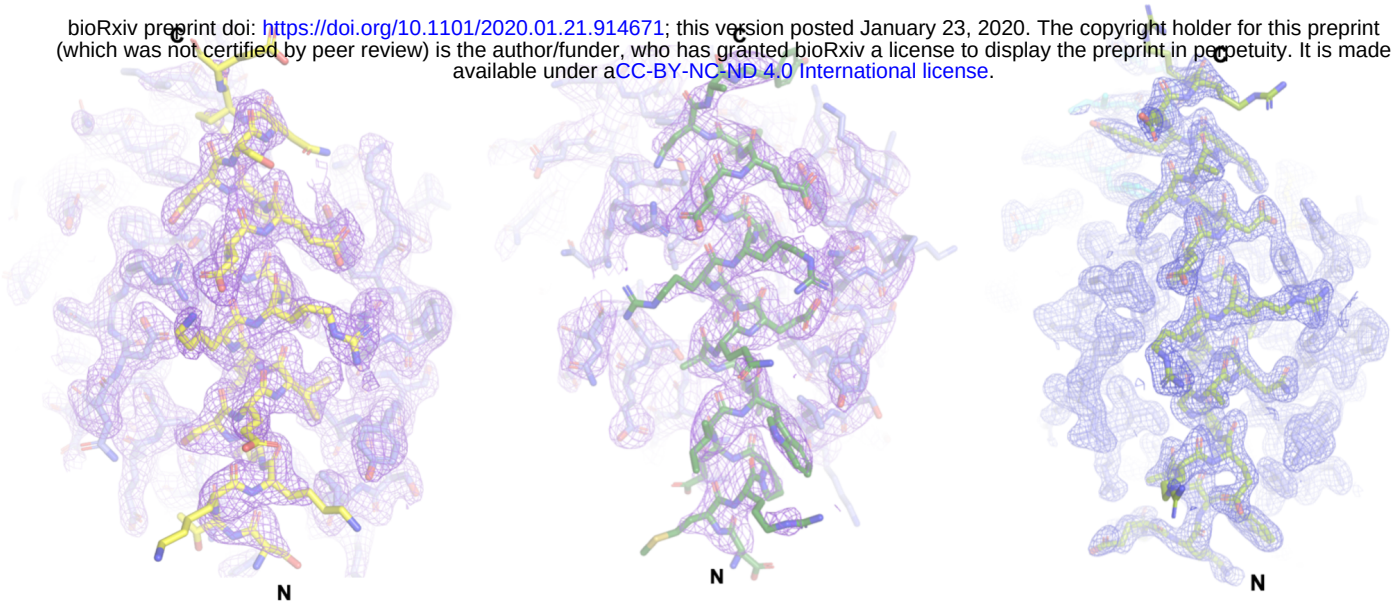

TPV16L:Bax BH3 **TPV16L:Bim BH3** **TPV16L:Puma BH3**

Figure S2